

Development of Aluminum-based Dissolvable Alloys for Hydraulic Fracturing Applications

Ezz Ahmed, Hani Henein, Ahmed Qureshi, Jing Liu

Abstract

Downhole tools made of dissolvable alloys (DAs) are getting more attractive, especially with the difficulties that arise from drilling wellbores with longer lateral distances. To date, most of the DAs are based on Al alloys (AAs) or Mg alloys, which offer undesirable mechanical properties. This work aims to develop a series of new Al-based DAs, providing high material strength and fast corrosion rates, for hydraulic fracturing applications. Given the enormous possibilities in tuning the structures and compositions of potential DAs, a literature review was first done to summarize the effects of various alloying elements on the microstructures, mechanical properties, and corrosion resistance of AAs. The main chemistry in downhole environments is KCl while the abundant electrochemical data of AAs are in NaCl electrolytes. In order to maximize the available electrochemical data of AAs, the effect of the associate cation type (K^+ vs. Na^+) on the corrosion of selected alloys was investigated by comparing the electrochemical values obtained under the same Cl^- molar concentration of KCl vs. NaCl solutions. To facilitate the design and elemental selection, Taguchi's method was utilized to change the chemistry of a commercial alloy (AA 7075) by adding various elements (such as Cu, Ga, Ag, Sn, In, Zn, Cr, and Zr). Scheil-Gulliver model was used to predict the potential phases formed as well as their amounts. Based on the review and simulation results, a few candidate alloys were targeted which were anticipated to potentially yield high mechanical properties and active corrosion behavior. It is believed that the experimental and simulation methods employed in the work will facilitate the development of the most promising DA compositions for downhole applications.

Keywords: Downhole tools; Dissolvable alloys (DAs); Al alloys (AAs); Material strength; Corrosion

1. Introduction

Multi-stage hydraulic fracturing by plug-and-perf is one of the most successful and economical methods for oil and gas extraction in unconventional reservoirs [1]. All plug-and-perf systems require frac plugs to isolate zones in the wellbore. Since hydraulic fracturing was developed on a commercial scale in 1949, the frac plug technology has undergone three distinct step changes based on the construction materials. Walton et al. [2] summarized these three stages into cast iron age (1950s through 1990s), composite age with the birth of the horizontal completion (1990s – Today), and Dissolvable Age – (2010s-Today). Traditional frac plugs are constructed from cast iron, composite materials, and non-dissolving elastomers. Once all fracturing stages are completed, traditional frac plugs must be removed from the wellbore with a coiled tubing unit to maximize production. The mill-out process is costly, problematic, risky, and can sometimes lead to production delays [3]. Inevitably, this inspired the idea of a dissolvable plug that would simply vanish, taking all of these problems with it [4].

Driven by efficiency needs and advancements in available materials, dissolvable materials are currently used to create dissolvable frac plugs (DFPs) that greatly reduced the need for milling with coiled tubing. At the end of 2017, roughly 2% of all frac plugs deployed in the field were made of dissolvable metals. The market is expected to grow to 5% of all frac plugs deployed in the field by the end of 2018 – a 250% growth in one year, with adoption and use increasing through 2025.[5] A DFP is made of dissolvable materials and designed in a way such that it will degrade completely to leave an unrestricted wellbore for production. Obviously, material selection is the key. The selected high-strength dissolvable metal must allow dissolution in water-based wellbore fluid, formation fluid, or production fluid [4]. Downhole chemistry and temperature are the two primary variables considered when determining the right material composition for dissolvability in any given application. Most alloys used in today's DFPs are Mg or Al-based, also requiring that the operator understand the exact chemistry of the well fluid to predictably estimate how long it will take for that plug to dissolve. However, downhole chemistry changes constantly. It varies dramatically from the vertical to the heel, and from heel to the toe. It varies from one well to the next, even on a multi-well pad. It's affected by the original water source and the fluid being pumped into the well. With so many variables, predicting how long it will take for the plug to dissolve is complicated. In turn, the material selection for desirable DFPs is complicated.

As a promising material, Al and Al alloys (AA) have favorable properties that if exploited properly, can yield the desired controlled dissolution and the necessary mechanical strength. Even though pure Al possesses desirable corrosion rates, Al is a soft, ductile, and relatively weak material to be utilized in the target downhole application [6].

The low strength can be compensated by alloying with other elements such as Mg, Zn, Cu, etc. AA 7075, 7050, and 7049 are AAs with high strength, among which AA 7075 possesses the highest strength [7]. The high mechanical properties of AA 7075 make it a good base material for the development of DA, yet its corrosion behavior needs to be adjusted to adapt to the targeted dissolvability in wellbore conditions. Another downside of AAs is the formation of stable protective oxide film formed on the surface, which in turn passivates its electrochemical (EC) activity. Al activation can be approached by (1) depassivation, i.e., alloying with low melting point metals (e.g., Ga, In, Sn and their respective low melting point intermetallic phases with Mg, Zn, etc.) [8], and (2) micro-galvanic corrosion, i.e., alloying with elements that trigger localized galvanic corrosion such as Ag [9]. The alloying elements' search space, as well as the elemental composition ranges, are huge. Furthermore, most corrosion data found in the literature are reported in NaCl electrolyte, while wellbore fluid has environments containing KCl solution – adding another challenge to overcome.

To address all the challenges in an efficient manner, in this work, firstly the effects of Cu, Mg, Zn, Ag, Ga, In, Sn, Cr, Er, and Zr on the mechanical properties and corrosion behavior of AAs were summarized to support our initial elemental selections and their composition ranges. Secondly, to extend the library of corrosion datasets, EC tests were performed to investigate the corrosion behavior of AA 7075, AA 6061, AA 2024, and dissolvable Al alloy in KCl and NaCl electrolytes at the same Cl⁻ molar concentration. Finally, Taguchi's method and Scheil-Gulliver's model were utilized to facilitate the material design, narrow the composition range and lead to future casting direction.

2. Alloying elements on the microstructures, mechanical properties, and corrosion of Al alloys: a review

Given the enormous possibilities in tuning the structures and compositions of potential DAs, a literature review is presented below to summarize the effects of various alloying elements on the microstructures, mechanical properties, and corrosion resistance of Al alloys. The alloying elements considered in this study are Ga, In, Sn, Mg, Zn, Cu, Ag, Cr, Er, and Zr. The selection was initially made based on the known effects those elements have on the mechanical properties as well as the electrochemical behavior of Al and Al alloys.

Gallium, Indium, and Tin – the activation of Al by adding Ga, In, and Sn has been investigated by several researchers [8, 10–12]. Woodall et al. (2011) [10] studied the effect of the liquid Ga-In-Sn (GIS) phase on a bulk AA [10]. The liquid GIS phase, with a melting point of 10.4 °C [13], is the key factor for the depassivation of Al-Ga-In-Sn alloy. It was confirmed that Al present in the liquid Ga or GIS phases first reacts with water. The consumed Al in the reaction causes a drop in Al equilibrium concentration, resulting in a chemical potential gradient as the driving force for Al diffusion from grains to maintain equilibrium. This in turn consumes Al atoms in the alloy as the hydrolysis reaction continues. On the other hand, intermetallic phases such as TiAl₃ and Al₂Cu do not involve in the reaction [12]. He et al. (2016) [11] studied the microstructure and interface reactions of Al-Ga-In-Sn alloys, with different In/Sn mass ratios [11]. It was concluded that the activation of Al did not necessarily take place in the presence of the GIS eutectic. Other GIS mixtures, Ga with β (In₃Sn) and γ (InSn₄), could also dominate Al activation at reaction temperatures, i.e., their respective melting points. Al-Ga-In-Sn alloy exhibits high reactivity with water at GIS eutectic composition at mass ratios of Ga:In:Sn = 65:22:13, thus, the alloys considered in this study has total GIS composition ranges of 1.5, 3, and 6 wt.%, at which a high activity is achieved [11, 14]. Nevertheless, it is believed that adding Ga, In, and Sn will increase the corrosion of AAs; the lower end of 1.5 wt.% GIS content is chosen here to address the concern of liquid embrittlement caused by those low melting point metals.

Magnesium – recently, the influence of alloying Mg in Al-Mg-Ga-In-Sn has been investigated [14–16]. According to the Al-Mg binary phase diagram [17], adding Mg greater than 2 wt.% enables the formation of β phase (Al₃Mg₂). The formation of β phase and other grain-boundary precipitates, in higher Mg content alloys, has been related to stress corrosion cracking (SCC). These precipitates can be developed slowly at ambient temperatures, or the process can be accelerated at a temperature in the range 37.78 – 176.67 °C. [18] Du et al. (2018) [14] examined the effects of varying Mg content in Al-xMg-3.8Ga-1.5In-0.7Sn with 2.4 wt.% Al-5Ti-1B as grain refiners. Binary phase diagrams predict the formation of MgIn, Mg₂Sn, MgGa₂, MgGa, MgGa₂, and Mg₅Ga₂ phases during solidification [19]. Interestingly, the formation of the In₃Sn phase reported previously [8, 11] was not observed when adding Mg in as-cast alloys. However, β In₃Sn was present in the rapidly solidified alloys regardless of Mg addition [16]. The appearance of β Al₃Mg₂ phase only occurred with Mg content at 5 wt.% and greater. Baer et al. (2000) [20] also concluded that the thickness of oxides remained unchanged, showing no impact on the dissolution of Al. Even though adding Mg could improve the mechanical properties of AAs. It potentially reduces the Al reactivity with water (i.e., reducing cathodic

sites) [21]. The base material chosen for this study, AA 7075, has 2.1-2.9 wt.% Mg. Therefore, Mg will not be considered as a design factor in this study.

Zinc – another way to interfere with the protective oxide films of Al is by adding Zn. Several studies reported the effectiveness of this method, especially in Al-air battery anode [22–25]. Zn addition in the Al electrode resulted in a more active potential in alkaline solutions, owing to the formation of Zn passive films [26]. Ternary Al-Zn-X alloys (where X is Ga, In, or Sn) have been shown to possess a more electronegative behavior. Al-Zn-Ga exhibits a ternary eutectic at 23 °C with the composition of Al-2Zn-14Ga [25]. Aragon et al (1996) [25] suggested that the mechanism for Al activation is similar to the liquid GIS eutectic discussed above. Venugopal and Raja (1997) [24] investigated the influence of In and Zn on the electrochemical behavior of Al-Zn-In alloy in a chloride medium. The researchers also observed In segregation owing to its low solubility in both Zn and Al according to their phase diagrams. This in turn promotes intergranular corrosion at In-rich and Zn-rich zones formed during solidification and surface diffusion. Further, similar behavior was observed by Khireche et al (2014) [23] in the study of Sn addition to Al-Zn alloy. Alloying Sn with Al-5Zn shifted the polarization curves to a more active position and increased the corrosion current density. No passive regions were observed in the Al-Zn-Sn alloys due to the active dissolution of Sn to Sn(OH)₂, SnO, and SnO₂ [27]. Unlike alloying with Mg, the addition of Zn to form Al-Zn-Ga-In-Sn alloy showed the presence of the In₃Sn phase [28]. However, the presence of Zn in grain boundaries dictates changes in Al and grain boundary phases (e.g., GIS phases) interactions. As Zn has a higher melting point than the other grain boundary phases, an increase in activation energy was confirmed causing a barrier for the hydrolysis reaction. Adding Zn up to 2 wt.% was reported to present no significant change in Al reactivity (i.e., micro-galvanic cells of Al-Zn compensate for the reduced effectiveness of GIS eutectic) while increasing Zn content up to 5 wt.% could decrease the dimensions of grain boundaries. The Al activity will then be hindered owing to the higher activation energy. [28] The Zn content in the base AA 7075 is 5.80 wt.%. zinc content will be adjusted for desirable Zn/Mg ratios. In addition, fixed Zn content in dissolvable Al and Mg alloys was reported to be 4-6 wt.% [23, 29–31]. This study will consider Zn content of 4 wt.% as a lower level (corresponding to Zn/Mg ratio of 1.67), and of 12 wt.% as a higher level (corresponding to Zn/Mg ratio of 5).

Copper – as Cu has low solubility in Al at low temperatures (maximum solubility of 5.7 wt.% Cu at 550 °C [17]), changes in intermetallic phases at grain boundaries, especially low melting point phases, are expected owing to the formation of Cu bearing intermetallics at grain boundaries. He et al (2019) [32] reported further increase in Cu content at grain boundaries occurred when Cu content increased up to 8 wt.%. In addition, they also found that the formation of θ (Al₂Cu) led to a decrease in Al grain size. This was explained by the role this phase play as a nucleation site during solidification, which in turn improves the mechanical properties. It was concluded that the addition of Cu to form Al-Cu-Ga-In-Sn alloys slowed the reaction as the θ (Al₂Cu) phase that occupies GIS sites, and decreases the Al-GIS contact area [32]. El Warraky et al. (2007) [33] investigated the impact of increasing the Cu content up to 11 wt.% on Al. It was shown that higher localized corrosion activity was obtained at higher Cu content. Moreover, Cu-bearing intermetallic phases such as S (Al₂CuMg) and Mg(ZnAlCu)₂ are susceptible to the de-alloying process in chloride solutions which further alter the corrosion behavior [34–36]. A wide range (4.1 – 11 wt.%) of Cu content would be considered in this study to show the influence of the amount and type of precipitates' phases on the corrosion and mechanical strength.

Silver – a small addition of Ag to AAs increases the mechanical strength through precipitation strengthening [37, 38]. In Al-Zn-Mg alloys, a small quantity of Ag reduces the width of precipitate free zones (PFZs) owing to the increased nucleation site density; thus, improving mechanical properties [37, 38]. Moreover, Ag and Sn have a dual effect on improving the tensile properties of Al-Zn-Mg alloys [37]. In terms of corrosion behavior, Ag, as a noble metal, accelerates corrosion on other active metals since it does not readily polarize. Thus, localized galvanic cells between Ag particles and Al matrix would form and enhance corrosion [39]. The influence of Ag content on the mechanical properties and corrosion behavior would be considered in a range between 0.07 and 4.2 wt.%. The lower level would reveal the influence on mechanical properties based on the discussion above, while the higher level would give insight into the localized galvanic corrosion behavior.

Chromium, Zirconium, and Erbium – the addition of Cr to Al not only reduces stress corrosion and improves toughness, but also controls grain structure and grain growth in Al-Mg-Si or Al-Mg-Zn alloys during heat treatment [40]. The intermetallic compounds are produced upon adding Cr and Zr to Al alloys, which also influence the corrosion behavior [38]. The addition of Cr will improve the corrosion resistance of AAs owing to the enhanced passivation due to the formed intermetallics as well as the increased Cr density in the solid solution [41]. H.C. Fang et al. (2014) [42] also studied the influence of alloying with Cr, Zr, and Er on the mechanical and electrochemical properties of Al-Zn-Mg-Cu alloys. They concluded that adding those alloying elements improved the mechanical and corrosion-resistant

behavior as they would restrict the recrystallization at grain boundaries. It was observed that adding 0.16 wt.% Zr resulted in Ultimate Tensile Strength (UTS) and Yield Strength (YS) of 704.0 and 683.6 MPa, respectively, while adding 0.16 wt.% Zr, 0.3 wt.% Er, and 0.18 wt.% Cr resulted in UTS and YS of 743.9 and 728.1 MPa, respectively. Alloying with Zr alone shifted the corrosion potential to the more active position and did not decrease the corrosion current density comparing with alloying with Zr, Er, and Cr together. AA 7075 has very few amounts of Cr and Zr, 0.19 and 0.02 wt.%, respectively. Therefore, Cr and Zr would be considered as grain refiners in this study, and their influence on mechanical properties would be studied up to 1 wt.% at a higher level.

In summary, this work would put the scope on the alloying elements influencing the dissolvability and mechanical properties of the targeted DA. The selected elements are:

- i) Ga, In, and Sn added at the GIS eutectic mass ratio of 68:22:13, respectively, and at the total composition of 1.5, 3, and 6 wt.%; expecting a boost in the corrosion rates of the designed alloys;
- ii) Cu and Zn having lower and higher levels of 4.1 – 11 wt.% and 4 – 12 wt.%, respectively, as well as Mg at a fixed composition of 2.4 wt.%; forming intermetallic phases which enhance the mechanical properties;
- iii) Ag in the range of 0.07 – 4.2 wt.%; forming micro-galvanic cells that enhance corrosion as well as improving mechanical properties via PFZs reduction;
- iv) Cr and Zr as grain refiners in amount up to 1 wt.%; expecting an increase in mechanical strength and control over grain growth and structure.

3. Methodology

3.1 Electrochemical experiments

Commercial AA 2024, AA 6061, AA 7075, and dissolvable Al (Table 1) were used in EC testing. Open circuit potential (OCP) and linear polarization resistance (LPR) measurements were performed using an EC potentiostat in aqueous NaCl and KCl solutions at the same Cl⁻ molar concentration. The wt.% concentration of KCl is 4.46 wt.%, which is calculated to be equivalent to 3.5 wt.% NaCl. The EC cell consisted of a three-electrode arrangement with the potential being recorded with respect to saturated Ag/AgCl reference electrode and graphite as a counter electrode. LPR tests were performed in voltage ranging from -0.1 V vs OCP to 0.1 V vs OCP at a scan rate of 0.5 mV/s.

Table 1 Compositions (wt.%) of selected Al alloys

Alloy	Zn	Mg	Cu	Ag	Ga	Cr	Fe	Si	Mn	Ti	Zr	V	Al
AA 2024	-	1.42	3.53	-	-	-	0.22	-	0.22	-	-	-	Bal.
AA 6061	0.05	1.00	0.32	-	-	-	0.50	0.73	0.03	-	-	-	Bal.
AA 7075	5.80	2.40	1.50	-	-	0.19	0.17	0.08	0.04	0.03	0.02	0.01	Bal.
Dissolvable Al	-	2.60	4.10	2.10	2.00	-	-	-	-	-	-	-	Bal.

3.2 Simulation of Alloy Phases

The chemical compositions of the designed alloys considered for phase simulation are shown in Table 1. Those alloys represent a systemic approach with L27 (6 design factors at 3 levels) orthogonal array of the Taguchi method. Thermo-Calc software was used to predict the intermetallic phases formed during solidification which would enhance the mechanical properties and boost the corrosion activity. The model used in the simulation is Scheil-Solidification, and the database used is TCAL7, a database designed for Al-based alloys.

Table 2 Composition (wt.%) of the designed DAs used in the simulation

DA	Cu	Zn	Mg	Ag	Ga	In	Sn	Cr	Zr	Ti	V	Al
1	4.10	4.00	2.40	0.70	0.88	0.37	0.25	0.19	0.00	0.03	0.01	87.07
2	4.10	4.00	2.40	0.70	0.88	0.37	0.25	0.60	0.50	0.03	0.01	86.16

3	4.10	4.00	2.40	0.70	0.88	0.37	0.25	1.00	1.00	0.03	0.01	85.26
4	4.10	8.00	2.40	2.14	1.75	0.75	0.50	0.19	0.00	0.03	0.01	80.13
5	4.10	8.00	2.40	2.14	1.75	0.75	0.50	0.60	0.50	0.03	0.01	79.22
6	4.10	8.00	2.40	2.14	1.75	0.75	0.50	1.00	1.00	0.03	0.01	78.32
7	4.10	12.00	2.40	4.20	3.80	1.50	0.70	0.19	0.00	0.03	0.01	71.07
8	4.10	12.00	2.40	4.20	3.80	1.50	0.70	0.60	0.50	0.03	0.01	70.16
9	4.10	12.00	2.40	4.20	3.80	1.50	0.70	1.00	1.00	0.03	0.01	69.26
10	7.55	4.00	2.40	2.14	3.80	1.50	0.70	0.19	0.50	0.03	0.01	77.18
11	7.55	4.00	2.40	2.14	3.80	1.50	0.70	0.60	1.00	0.03	0.01	76.27
12	7.55	4.00	2.40	2.14	3.80	1.50	0.70	1.00	0.00	0.03	0.01	76.87
13	7.55	8.00	2.40	4.20	0.88	0.37	0.25	0.19	0.50	0.03	0.01	75.62
14	7.55	8.00	2.40	4.20	0.88	0.37	0.25	0.60	1.00	0.03	0.01	74.71
15	7.55	8.00	2.40	4.20	0.88	0.37	0.25	1.00	0.00	0.03	0.01	75.31
16	7.55	12.00	2.40	0.70	1.75	0.75	0.50	0.19	0.50	0.03	0.01	73.62
17	7.55	12.00	2.40	0.70	1.75	0.75	0.50	0.60	1.00	0.03	0.01	72.71
18	7.55	12.00	2.40	0.70	1.75	0.75	0.50	1.00	0.00	0.03	0.01	73.31
19	11.00	4.00	2.40	4.20	1.75	0.75	0.50	0.19	1.00	0.03	0.01	74.17
20	11.00	4.00	2.40	4.20	1.75	0.75	0.50	0.60	0.00	0.03	0.01	74.76
21	11.00	4.00	2.40	4.20	1.75	0.75	0.50	1.00	0.50	0.03	0.01	73.86
22	11.00	8.00	2.40	0.70	3.80	1.50	0.70	0.19	1.00	0.03	0.01	70.67
23	11.00	8.00	2.40	0.70	3.80	1.50	0.70	0.60	0.00	0.03	0.01	71.26
24	11.00	8.00	2.40	0.70	3.80	1.50	0.70	1.00	0.50	0.03	0.01	70.36
25	11.00	12.00	2.40	2.14	0.88	0.37	0.25	0.19	1.00	0.03	0.01	69.73
26	11.00	12.00	2.40	2.14	0.88	0.37	0.25	0.60	0.00	0.03	0.01	70.32
27	11.00	12.00	2.40	2.14	0.88	0.37	0.25	1.00	0.50	0.03	0.01	69.42

4. Results and discussion

4.1 The effect of associate cations S (K^+ vs. Na^+) on the corrosion of selected materials

Equilibrium OCP values, i.e., corrosion potentials (E_{Corr}) of mechanically polished AA 2024, AA 6061, AA 7075, and dissolvable Al electrodes in 3.5 wt.% NaCl and 4.46 wt.% KCl (table 3) reveal insignificant variance upon changing cation type for each material. Fig. 1 presents the obtained E_{Corr} and corrosion current densities (i_{Corr}). ANOVA results further assure the insignificance effect of changing cation type (Na^+ vs K^+), where the P-Values (0.981 and 0.889 for i_{Corr} and E_{Corr} , respectively) are greater than the level of significance ($\alpha = 0.05$). Thus, the null hypothesis of equal means $H_0: \mu_1 = \mu_2$ is not rejected. This can be explained by the similar chemical combining activity of both electrolytes. The selected cations' impact on corrosion has also been reported in other studies [43, 44], where Na^+ and K^+ cations were reported to have relatively small effects on corrosion. Therefore, it is reasonable to conclude that metals behave the same in NaCl and KCl solutions of similar milliequivalents.

Table 3 OCP values of selected alloys in 3.5 wt.% NaCl and 4.46 wt.% KCl at room temperature

Alloy	Cation	OCP (mV vs Ag/AgCl)
AA 2024	K+	-576
	Na+	-555
AA 6061	K+	-710
	Na+	-705
AA 7075	K+	-781
	Na+	-768
Dissolvable Al	K+	-1,209
	Na+	-1,220

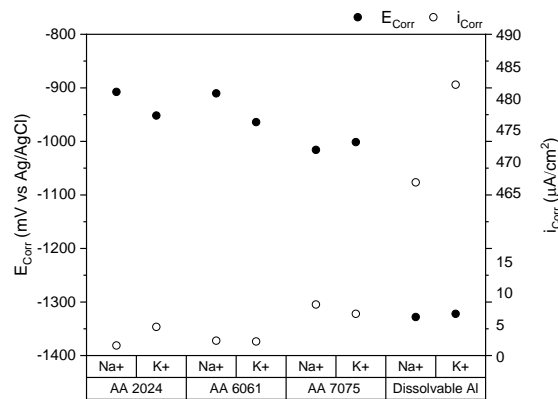


Fig. 1 EC results for commercial AAs in 3.5 wt.% NaCl vs. 4.46 wt.% KCl solutions at room temperature. a) Box plot illustrating differences in means and ranges of OCP values (mV. vs Sat'd Ag/AgCl), b) the influence of Na⁺ and K⁺ cations on the corrosion potential and corrosion current density

4.2 Prediction of intermetallic phases formed during solidification

Fig. 2 shows the compositions of main phases with respect to the 27 designed DAs in Table 2 predicted by Thermo-Calc. It can be seen that the major intermetallic phases found in the 7xxx series of AAs, i.e. η ($MgZn_2$), S (Al_2CuMg), and θ (Al_2Cu) are present in varying amounts depending on the alloy composition [45, 46]. In addition, Z phase (i.e., Mg_2Zn_{11} or $Al_5Cu_6Mg_2$ [45]), Mg_2Sn , and BCC phase (i.e., dispersed Ag) are also present. It is reported that mechanical properties including strength, toughness, SCC resistance are largely influenced by η , S, and θ phases [ref], while Mg_2Sn and BCC Ag have a nobler corrosion potential compared to pure Al [14]. In this work, more interest and attention are paid on the η and Z phases because they will not only lead to high corrosion activity of AAs but also contribute to mechanical properties enhancement[47].

The amount of η phase is high in DAs 4-6,11, and 21-24; Z phase content is high in alloys 13, 18, 25, and 27; Mg_2Sn content is high in alloys 7-9 and 22-24. Although θ phase enhances the mechanical properties of Al alloys, it alters Al depassivation by changing the chemistry of GIS mixtures at grain boundaries and their contact area with Al grains; θ phase is high in DAs 20-24, which should be excluded for the initial investigation. Thus, the initial alloys which are expected to yield favorable results in terms of dissolvability and mechanical properties are DAs 13, 25, and 27, where the θ and η phase contents are moderate and Z phase is high. In terms of favorable corrosion behavior, DA 18 has a high amount of Z phase and a moderate amount of η phase with low θ intermetallics. It is suspected that a critical conclusion will be drawn on the influence of θ phase on corrosion and mechanical properties of AAs by comparing DA 18 with DAs 25 and 27. Unfortunately, our current attempt failed to simulate the solidification process for DAs 16, 17, 19, and 26; further investigation is part of the ongoing research.

It is expected that the selected alloys (DAs 13, 18, 25, and 27) will exhibit high yield strength and hardness due to the presence of the coarse η and Z phases. The presence of coarse intermetallic phases in as-cast alloys potentially causes embrittlement, thus the ductility is expected to be at its lowest. Embrittlement in AA 7075 due to coarse intermetallic phases have been reported in another study [47], which can be treated by homogenization. Liquid embrittlement caused by the presence of low melting point intermetallics could also affect the mechanical properties of the alloys. DAs 13, 25, and 27 only contain 1.5 wt.% of low melting point metals, therefore, the corresponding effects are suspected to be minimal. Future experimental investigation will be conducted to confirm the prediction of intermetallic phases in Fig. 2, and the corresponding corrosion and mechanical properties.

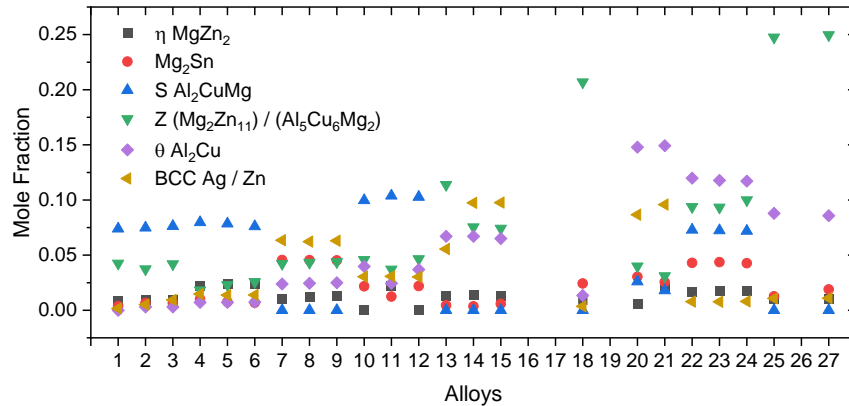


Fig. 2 Mole fractions of phases in each alloy predicted using TCAL7 database (Thermo-Calc 2021b)

5. Conclusion

In order to develop novel Al-based alloys with high material strength and fast corrosion rates, a preliminary investigation was carried out on reviewing the effects of various alloying elements, investigating the effect of the associate cations (K^+ vs. Na^+) on the corrosion of AAs, and the prediction of intermetallic phases formed during solidification. AA 7075 was selected as a base alloy owing to its excellent mechanical properties. In summary, the following conclusions are drawn:

- Effects of various alloying elements: i) Ga, In, and Sn influence the hydrolysis reaction of Al. This is due to the low melting point intermetallic phases formed that act as a pathway for Al atoms to diffuse into the aqueous environment; ii) The addition of Mg, Cu, and Zn into Al-Ga-In-Sn alloys not only changes the GIS chemistry at the grain boundaries but also reduces the contact area between Al grains and GIS eutectic/mixtures, which could be used as a controlling feature for the dissolution process. Besides, their intermetallic phases have a significant influence on the mechanical properties of AAs; iii) The addition of Ag in small quantities enhances the mechanical properties through the reduction of PFZs. Further, the noble corrosion potential of Ag will contribute to creating localized galvanic corrosion cells that fasten the dissolution process; iv) Further enhancement in DAs' mechanical properties could be achieved by the addition of Cr and Zr grain refiners.
- The insignificance of cation type (Na^+ vs K^+) was experimentally proven. It is, therefore, possible to expand the corrosion database by adopting published values in NaCl solution from literature.
- Prediction of intermetallic phases formed during solidification: i) simulation results reveal the formation of η ($MgZn_2$), S (Al_2CuMg), and θ (Al_2Cu) phases which are commonly found in the AA 7xxx series on which the high mechanical performance can be attributed. Z, BCC Ag, and Mg_2Sn phases will also be formed, which are more electrochemically active than AA 7075. Considering the effects of these phases in terms of dissolvability and mechanical properties, DAs 13, 18, 25, and 27 are anticipated to be the best candidates for manufacturing DFPs in hydraulic fracturing.

It is believed that the experimental and simulation methods employed in the work will facilitate the development of the most promising DA composition with a unique combination of high strength and desirable corrosion rate in downhole environments. Further research is needed to assess the conclusions drawn from this study by experimental validation. The selected alloys will be cast, and microstructure, electrochemical, and mechanical testing will be performed accordingly.

Acknowledgements

The authors would like to acknowledge the financial support of the Natural Sciences and Engineering Research Council of Canada (NSERC), and the Hadhramout Foundation for Mr. Ezz Ahmed's MSc study.

References

1. Xu DJ, Liao RQ, Li ZW, et al (2015) Research on Productivity for Multi-stage Fracturing of Horizontal Wells. *Chem Eng Trans* 46:1189–1194. <https://doi.org/10.3303/CET1546199>
2. Walton Z, Fripp M, Porter J, Vargus G (2019) Evolution of Frac Plug Technologies – Cast Iron to Composites to Dissolvable. In: SPE Middle East Oil and Gas Show and Conference, MEOS, Proceedings. OnePetro
3. Garcilazo Meza G, Bautista Alarcon X, Loundy R (2020) A Detailed Evaluation of Coiled Tubing Drillouts of Composites and Dissolvable Plugs In Permian Basin and Eagle Ford Fields. In: Society of Petroleum Engineers - SPE/ICoTA Well Intervention Conference and Exhibition 2020, CTWI 2020. OnePetro
4. Fripp M, Walton Z (2016) Degradable metal for use in a fully dissolvable frac plug. In: Proceedings of the Annual Offshore Technology Conference. Offshore Technology Conference, pp 3467–3475
5. ASM International (2018) Terves to expand magnesium foundry for manufacturing dissolvable metal tools - ASM International. https://www.asminternational.org/home/-/journal_content/56/10180/35028237/NEWS. Accessed 14 Aug 2021
6. Megson THG (2019) Introduction. In: Structural and Stress Analysis, Fourth Edition. Butterworth-Heinemann, pp 1–16
7. Hirsch J (2011) Aluminium sheet fabrication and processing. In: Roger Lumley (ed) Fundamentals of Aluminium Metallurgy: Production, Processing and Applications. Woodhead Publishing, pp 719–746
8. Wang W, Zhao XM, Chen DM, Yang K (2012) Insight into the reactivity of Al-Ga-In-Sn alloy with water. *Int J Hydrogen Energy* 37:2187–2194. <https://doi.org/10.1016/j.ijhydene.2011.10.058>
9. Fripp M, Walton Z, Norman T (2017) Fully dissolvable fracturing plug for low-temperature wellbores. In: Proceedings - SPE Annual Technical Conference and Exhibition. Society of Petroleum Engineers (SPE)
10. Ziebarth JT, Woodall JM, Kramer RA, Choi G (2011) Liquid phase-enabled reaction of Al–Ga and Al–Ga–In–Sn alloys with water. *Int J Hydrogen Energy* 36:5271–5279. <https://doi.org/10.1016/J.IJHYDENE.2011.01.127>
11. He TT, Wang W, Chen W, et al (2017) Influence of In and Sn compositions on the reactivity of Al–Ga–In–Sn alloys with water. *Int J Hydrogen Energy* 42:5627–5637. <https://doi.org/10.1016/J.IJHYDENE.2016.11.112>
12. Trenikhin M V., Bubnov A V., Nizovskii AI, Duplyakin VK (2006) Chemical interaction of the In-Ga eutectic with Al and Al-base alloys. *Inorg Mater* 42:256–260. <https://doi.org/10.1134/S0020168506030083>
13. Villars P, Prince A OH (1997) In: Al-In-Sn phase diagram. In: Handbook of ternary alloy phase diagrams, 2nd ed. ASM International, pp 11045–11045
14. Du BD, He TT, Liu GL, et al (2018) Al-water reactivity of Al–Mg–Ga–In–Sn alloys used for hydraulic fracturing tools. *Int J Hydrogen Energy* 43:7201–7215. <https://doi.org/10.1016/j.ijhydene.2018.02.090>
15. Bangdeng D, Jun L, Xiaowan W, et al (2021) Effect of Heat Treatment on Microstructure and Al-water Reactivity of Al-Mg-Ga-In-Sn Alloys. *Chinese J Mater Res* 35:25–35. <https://doi.org/10.11901/1005.3093.2020.080>
16. He T, Chen W, Wang W, et al (2020) Microstructure and hydrogen production of the rapidly solidified Al–Mg–Ga–In–Sn alloy. *J Alloys Compd* 827:154290. <https://doi.org/10.1016/J.JALLCOM.2020.154290>
17. H. Okamoto; M.E. Schlesinger; E.M. Mueller (2016) Al (Aluminum) Binary Alloy Phase Diagrams. In: Alloy Phase Diagrams. ASM International, pp 113–139
18. Speidel MO, Hyatt M V. (1972) Stress-Corrosion Cracking of High-Strength Aluminum Alloys. In: Mars G. Fontana, Roger W. Staehle (eds) Advances in Corrosion Science and Technology. Springer, Boston, MA, Boston, MA, pp 115–335
19. H. Okamoto; M.E. Schlesinger; E.M. Mueller (2016) Binary Alloy Phase Diagrams. In: Alloy Phase Diagrams. ASM International, pp 89–89
20. Baer DR, Windisch CF, Engelhard MH, et al (2000) Influence of Mg on the corrosion of Al. *J Vac Sci Technol A Vacuum, Surfaces, Film* 18:131–136. <https://doi.org/10.1116/1.582129>
21. Ghali E (2010) Corrosion resistance of aluminum and magnesium alloys : understanding, performance, and testing. John Wiley

22. Hong MS, Park IJ, Kim JG (2017) Alloying effect of copper concentration on the localized corrosion of aluminum alloy for heat exchanger tube. *Met Mater Int* 23:708–714. <https://doi.org/10.1007/s12540-017-6589-9>
23. Khireche S, Boughrara D, Kadri A, et al (2014) Corrosion mechanism of Al, Al-Zn and Al-Zn-Sn alloys in 3wt.% NaCl solution. *Corros Sci* 87:504–516. <https://doi.org/10.1016/j.corsci.2014.07.018>
24. Venugopal A, Raja VS (1997) AC impedance study on the activation mechanism of aluminium by indium and zinc in 3.5% NaCl medium. *Corros Sci* 39:2053–2065. [https://doi.org/10.1016/S0010-938X\(97\)00082-6](https://doi.org/10.1016/S0010-938X(97)00082-6)
25. Aragon E, Cazenave-Vergez L, Lanza E, et al (1997) Electrochemical behaviour of binary Al-Ga and ternary Al-Zn-Ga alloys as function of thermodynamic properties. *Br Corros J* 32:121–126. <https://doi.org/10.1179/000705997798115011>
26. Macdonald DD, Ismail KM, Sikora E (1998) Characterization of the Passive State on Zinc. *J Electrochem Soc* 145:3141. <https://doi.org/10.1149/1.1838777>
27. Ahmido A, Sabbar A, Zouihri H, et al (2011) Effect of bismuth and silver on the corrosion behavior of Sn–9Zn alloy in NaCl 3 wt.% solution. *Mater Sci Eng B* 176:1032–1036. <https://doi.org/10.1016/J.MSEB.2011.05.034>
28. Liu D, Gao Q, An Q, et al (2020) Experimental Study on Zn-Doped Al-Rich Alloys for Fast on-Board Hydrogen Production. *Cryst* 2020, Vol 10, Page 167 10:167. <https://doi.org/10.3390/CRYST10030167>
29. Flamini DO, Saidman SB (2012) Electrochemical behaviour of Al-Zn-Ga and Al-In-Ga alloys in chloride media. *Mater Chem Phys* 136:103–111. <https://doi.org/10.1016/j.matchemphys.2012.06.036>
30. Liu L, Yu S, Liu E, et al (2021) Effect of Ni addition on the mechanical and degradation properties of hollow glass microsphere/Mg alloy composites. *J Alloys Compd* 853:157125. <https://doi.org/10.1016/j.jallcom.2020.157125>
31. Liu L, Yu S, Liu E, et al (2021) Investigations on the Microstructure and Degradation Behavior of Hollow Glass Microspheres/Mg Alloy Composites. *Adv Eng Mater* 23:1–11. <https://doi.org/10.1002/adem.202001301>
32. He T, Chen W, Wang W, et al (2020) Effect of different Cu contents on the microstructure and hydrogen production of Al–Cu-Ga-In-Sn alloys for dissolvable materials. *J Alloys Compd* 821:153489. <https://doi.org/10.1016/j.jallcom.2019.153489>
33. El Warraky AA, El-Aziz AM, Soliman KA (2007) Copper redeposition and surface enrichment during the dissolution of Al-Cu alloys in different concentrations of NaCl solution. Part 1 - Electrochemical measurements. *Anti-Corrosion Methods Mater* 54:155–162. <https://doi.org/10.1108/00035590710748623>
34. Ramgopal T, Schmutz P, Frankel GS (2001) Electrochemical Behavior of Thin Film Analogs of Mg (Zn, Cu, Al) 2. *J Electrochem Soc* 148:B348. <https://doi.org/10.1149/1.1386626>
35. Meng Q, Frankel GS (2004) Effect of Cu Content on Corrosion Behavior of 7xxx Series Aluminum Alloys. *J Electrochem Soc* 151:B271. <https://doi.org/10.1149/1.1695385>
36. Buchheit RG, Martinez MA, Montes LP (2000) Evidence for Cu Ion Formation by Dissolution and Dealloying the Al₂CuMg Intermetallic Compound in Rotating Ring-Disk Collection Experiments. *J Electrochem Soc* 147:119. <https://doi.org/10.1149/1.1393164>
37. Ogura T, Hirose A, Hirose A, Sato T (2011) Effects of microalloying tin and combined addition of silver and tin on the formation of precipitate free zones and mechanical properties in Al-Zn-Mg alloys. In: *Materials Transactions. The Japan Institute of Metals and Materials*, pp 900–905
38. Ogura T, Otani T, Hirose A, Sato T (2013) Improvement of strength and ductility of an Al-Zn-Mg alloy by controlling grain size and precipitate microstructure with Mn and Ag addition. *Mater Sci Eng A* 580:288–293. <https://doi.org/10.1016/j.msea.2013.05.025>
39. Gudić S, Smoljko I, Kličić M (2010) The effect of small addition of tin and indium on the corrosion behavior of aluminium in chloride solution. *J Alloys Compd* 505:54–63. <https://doi.org/10.1016/j.jallcom.2010.06.055>
40. Fayomi OSI, Popoola API, Udoye NE (2017) Effect of Alloying Element on the Integrity and Functionality of Aluminium-Based Alloy. *Alum Alloy - Recent Trends Process Charact Mech Behav Appl*. <https://doi.org/10.5772/intechopen.71399>
41. Gupta RK, Fabijanic D, Zhang R, Birbilis N (2015) Corrosion behaviour and hardness of in situ consolidated nanostructured Al and Al-Cr alloys produced via high-energy ball milling. *Corros Sci* 98:643–650. <https://doi.org/10.1016/j.corsci.2015.06.011>
42. Fang HC, Chao H, Chen KH (2014) Effect of Zr, Er and Cr additions on microstructures and properties of Al-Zn-Mg-Cu alloys. *Mater Sci Eng A* 610:10–16. <https://doi.org/10.1016/j.msea.2014.05.021>
43. Hansson CM, Frølund T, Markussen JB (1985) The effect of chloride cation type on the corrosion of steel

- in concrete by chloride salts. *Cem Concr Res* 15:65–73. [https://doi.org/10.1016/0008-8846\(85\)90009-2](https://doi.org/10.1016/0008-8846(85)90009-2)
44. Tuutti K (1982) Corrosion of steel in concrete. Ph.D. Thesis. Swedish Cement and Concrete Research Institute, Stockholm
 45. X.-M. L, Starink MJ (2013) Effect of compositional variations on characteristics of coarse intermetallic particles in overaged 7000 aluminium alloys. <http://dx.doi.org/10.1179/026708301101509449> 17:1324–1328. <https://doi.org/10.1179/026708301101509449>
 46. Mondal C, Mukhopadhyay AK (2005) On the nature of T(Al₂Mg₃Zn₃) and S(Al₂CuMg) phases present in as-cast and annealed 7055 aluminum alloy. *Mater Sci Eng A* 391:367–376. <https://doi.org/10.1016/J.MSEA.2004.09.013>
 47. Ghosh A, Ghosh M (2018) Microstructure and texture development of 7075 alloy during homogenisation. <https://doi-org.login.ezproxy.library.ualberta.ca/101080/1478643520181439596> 98:1470–1490. <https://doi.org/10.1080/14786435.2018.1439596>